Cancer Research

IL6 Trans-signaling Promotes KRAS-Driven Lung Carcinogenesis

Gavin D. Brooks[1], Louise McLeod[1], Sultan Alhayyani[1], Alistair Miller[1], Prudence A. Russell[2,3], Walter Ferlin[4], Stefan Rose-John[5], Saleela Ruwanpura[1], and Brendan J. Jenkins[1]

Abstract

Oncogenic KRAS mutations occur frequently in lung adenocarcinoma. The signaling pathways activated by IL6 promote Kras-driven lung tumorigenesis, but the basis for this cooperation is uncertain. In this study, we used the *gp130*$^{F/F}$ (Il6st) knock-in mouse model to examine the pathogenic contribution of hyperactivation of the STAT3 arm of IL6 signaling on KRAS-driven lung tumorigenesis. Malignant growths in the *gp130*$^{F/F}$:*Kras*^{G12D} model displayed features of atypical adenomatous hyperplasia, adenocarcinoma *in situ*, and invasive adenocarcinoma throughout the lung, as compared with parental *Kras*^{G12D} mice, where STAT3 was not hyperactivated. Among IL6 family cytokines, only IL6 was upregulated in the lung. Accordingly, normalization of pulmonary STAT3 activity, by genetic ablation of either Il6 or Stat3, suppressed the extent of lung cancer in the model. Mechanistic investigations revealed elevation in the lung of soluble IL6 receptor (sIL6R), the key driver of IL6 trans-signaling, and blocking this mechanism via interventions with an anti-IL6R antibody or the inhibitor sgp130Fc ameliorated lung cancer pathogenesis. Clinically, expression of IL6 and sIL6R was increased significantly in human specimens of lung adenocarcinoma or patient serum. Our results offer a preclinical rationale to clinically evaluate IL6 trans-signaling as a therapeutic target for the treatment of KRAS-driven lung adenocarcinoma. *Cancer Res; 76(4); 866–76. ©2016 AACR.*

Introduction

Lung adenocarcinoma is the most common (∼40%) form of lung cancer, the number one cancer killer worldwide, which accounts for approximately 1.5 million deaths annually (1). Lung adenocarcinoma is often diagnosed at an advanced stage, and current treatment options largely comprising surgery, chemotherapy, and/or radiotherapy remain associated with a high risk of tumor reoccurrence and poor patient survival rates (5-year relative survival rate is ∼15%; ref. 2). The identification of EGFR-activating mutations in 15% to 20% of lung adenocarcinoma patients, mainly nonsmoking Asian females, has paved the way for targeted therapy with tyrosine kinase inhibitors (3). However, effective therapies for lung adenocarcinoma with more typical mutation profiles, namely those associated with cigarette smoking, which accounts for 80% to 90% of lung adenocarcinoma cases (2), remain to be identified, thus highlighting the need for a better understanding of the molecular and genetic alterations that promote the initiation and progression of lung adenocarcinoma.

One of the most extensively studied oncogenes implicated in lung carcinogenesis is *Kras*. Activating *KRAS* mutations are found in 10% to 40% of human lung adenocarcinoma (4, 5), with nearly all mutations occurring in codons 12 and 13 (6). A causal role for Kras in driving lung adenocarcinoma is evidenced by the spontaneous development of lung adenocarcinoma in mice genetically engineered to conditionally express the oncogenic *Kras*^{G12D} allele in the airway epithelium (7, 8). However, attempts to therapeutically target Kras for clinical benefit have been unsuccessful, and there is now a pressing need to identify "druggable" co-operating partners of oncogenic Kras.

It has recently emerged that oncogenic Kras engages cytokine signaling cascades to promote lung adenocarcinoma (9), although the identity of specific cytokines and the mechanistic basis by which they promote Kras-driven lung carcinogenesis remain ill-defined. The IL6 cytokine family includes protumorigenic cytokines IL6, IL11, oncostatin-M (OSM), and leukemia-inhibitory factor (LIF; refs. 10–15), and among these, IL6 has recently been reported to promote *Kras*^{G12D}-driven lung and pancreatic tumorigenesis (16–18). In the context of human lung adenocarcinoma, elevated systemic and pulmonary productions of IL6 are commonly observed in lung adenocarcinoma patients and correlate with poor patient survival (19–22). In addition, polymorphisms in the *IL6* gene are linked to increased lung cancer risk (23). IL6 transduces intracellular signals via two distinct modes: classical signaling via its membrane-bound (m) IL6 receptor (IL6R) and trans-signaling via a naturally occurring soluble (s) IL6R (24). In either case, IL6 transduces signals via the ubiquitously-expressed gp130 coreceptor, with the main downstream signaling mediator being the latent transcription factor signal transducer and activator of transcription (STAT)3 (25). Because mIL6R expression is restricted mainly to hepatocytes, intestinal epithelial cells, and subsets of leukocytes, sIL6R not only affords mIL6R^{-}gp130^{+}

[1]Centre for Innate Immunity and Infectious Diseases, Hudson Institute of Medical Research, Monash University, Clayton, Victoria, Australia. [2]St Vincent's Hospital, Fitzroy, Victoria, Australia. [3]Department of Pathology, Melbourne Medical School, Melbourne University, Parkville, Victoria, Australia. [4]NovImmune SA, Geneva, Switzerland. [5]Institute of Biochemistry, Christian-Albrechts-University, Kiel, Germany.

Note: Supplementary data for this article are available at Cancer Research Online (http://cancerres.aacrjournals.org/).

Corresponding Author: Brendan J. Jenkins, Hudson Institute of Medical Research, 27-31 Wright Street, Clayton, Victoria 3168, Australia. Phone: 61-3-9902-4708; Fax: 61-3-9594-7235; E-mail: brendan.jenkins@hudson.org.au

doi: 10.1158/0008-5472.CAN-15-2388

cells' (e.g., epithelial) responsiveness to IL6, but also potentiates the existing IL6 responsiveness of mIL6R$^+$gp130$^+$ cells. Collectively, these observations provide a rational explanation as to why IL6 classical signaling primarily regulates the humoral immune and hepatic acute phase responses to protect the host against tissue injury and/or infection, whereas exacerbation of IL6 trans-signaling has been implicated in the pathogenesis of inflammatory disorders (26–28), as well as colon and pancreatic cancers (15, 16, 29).

To identify IL6 family cytokines that promote Kras-driven lung adenocarcinoma, here we have coupled the Cre recombinase–inducible *Kras*$^{G12D/+}$ lung adenocarcinoma mouse model (7) with *gp130*$^{F/F}$ mice, the latter harboring a knock-in tyrosine (Y) to phenylalanine (F) mutation at residue 757 in gp130, which abrogates suppressor of cytokine signaling (SOCS)3–mediated downmodulation of IL6 cytokine family/STAT3 signaling (30, 31). We report that compared with control *Kras*^{G12D} mice, at 6 weeks after activation of oncogenic *Kras*, compound mutant *gp130*$^{F/F}$:*Kras*^{G12D} mice displayed an exacerbated lung adenocarcinoma phenotype, which correlated with enhanced lung cellular proliferation. Among IL6 family cytokines, only IL6 was upregulated in the lungs of *gp130*$^{F/F}$:*Kras*^{G12D} mice, and lung adenocarcinoma severity in *gp130*$^{F/F}$:*Kras*^{G12D} mice was suppressed by either homozygous or heterozygous ablation of *Il6* or *Stat3*, respectively, which returns augmented STAT3 activation levels in the lung back to normal (30, 32). Notably, sIL6R levels were elevated in the lungs of *gp130*$^{F/F}$:*Kras*^{G12D} mice, and the specific blockade of IL6 trans-signaling using genetic and antibody-mediated approaches ameliorated the exacerbated lung adenocarcinoma phenotype in *gp130*$^{F/F}$:*Kras*^{G12D} mice. In support of these observations, significantly increased protein expression of IL6 and sIL6R was also observed in human lung adenocarcinoma patient biopsies and sera. Collectively, these data reveal that IL6 trans-signaling promotes Kras-driven lung adenocarcinoma, and thus may provide a new therapeutic avenue for the treatment of human lung adenocarcinoma.

Materials and Methods

Human biopsies

Serum and lung tissue (from resection surgery) were collected from lung adenocarcinoma patients and control lung adenocarcinoma–free individuals (Supplementary Table S1), and snap-frozen in liquid nitrogen prior to molecular analyses. All samples were collected upon formal written informed consent, and studies were approved by the Monash Health Human Research Ethics Committee.

Cell lines and cell growth assays

Human lung adenocarcinoma cell lines A549 and NCI-H23 were maintained in DMEM (Invitrogen) supplemented with 10% heat-inactivated FCS (JRH Biosciences). Cell lines obtained directly from the ATCC were further characterized/authenticated via short tandem repeat profiling, and passaged in our laboratory for under 6 months after receipt. For cell growth assays, 0.5×10^3 cells were seeded into triplicate wells (96-well plates) with DMEM containing sgp130Fc (10 ng/mL). After 2 and 4 days of culture, 0.2 mg/mL of 3-(4,5-dimethylthiazol-2-yl)-2,5-diphenyl tetrazolium bromide (MTT; Sigma-Aldrich) reagent was added, following which, cells were incubated for a further 4 hours prior to solubilization of crystals with dimethyl sulfoxide. Absorbance was measured using a FLUROstar Optima plate-reader (BMG Labtech) at 560 nm.

Mice

The *gp130*$^{F/F}$, *gp130*$^{F/F}$:*Stat3*$^{-/+}$, *gp130*$^{F/F}$:*Il6*$^{-/-}$, *Il6*$^{-/-}$, and *sgp130Fc*^{Tg} mice have been previously reported (13, 30, 33, 34) and were back-crossed onto a *Kras*$^{G12D/+}$ background (7). Male and female mice were housed under specific pathogen-free conditions, and experiments were approved by the Monash University Animal Ethics committee.

Mouse treatments

Mice aged 6 weeks received adenoviral Cre recombinase (5×10^6 plaque-forming units; University of Iowa; ref.8) or, as a control, equivalent volume (125 μL) of PBS, by intranasal inhalation, and were observed for a further 6 weeks. The anti-IL6R mAbs 25F10 and 1F7, and IgG control (35, 36), were administrated to mice at 10 mg/kg by intraperitoneal injection twice weekly for 6 weeks, with the initial injection given the day after Cre inhalation.

Mouse histology and immunohistochemistry

The collection of mouse lungs for histologic evaluation by staining with hemotoxylin and eosin (H&E), as well as immunohistochemistry to detect CD45, thyroid transcription factor (TTF)-1, phosphotyrosine (pY)-STAT3 and proliferating cell nuclear antigen (PCNA), and terminal deoxynucleotidyl transferase (tdT)–mediated dUDP nick-end labeling (TUNEL) assay, was performed as before (30, 37). To quantify cellular staining within lungs, digital images of photomicrographs (100× high-power fields) were viewed using Image J software (National Institutes of Health). Positive-staining cells were counted manually ($n = 20$ fields) within a grid that was placed over photomicrographs with a random offset.

ELISA and immunoblotting

Total protein lysates were prepared from snap-frozen lung tissue and subjected to ELISA and immunoblotting. Mouse IL6 and human IL6 ELISA sets were purchased from BD Biosciences, whereas sIL6R and sgp130 ELISA sets were purchased from R&D Systems. Immunoblotting with antibodies against sIL6R (R&D Systems), pY-STAT3 and total STAT3 (Santa Cruz Biotechnology), and actin (Sigma-Aldrich) was performed on lung lysates, and protein bands were visualized using the Odyssey Infrared Imaging System (LI-COR) and quantified using Image J.

RNA isolation and gene expression analyses

Total RNA was isolated from snap-frozen mouse and human lung tissues, and quantitative RT-PCR (qPCR) was performed on cDNA with SYBR Green (Life Technologies) using the 7900HT Fast RT-PCR System (Applied Biosystems). Gene expression data acquisition and analyses were performed using the Sequence Detection System Version 2.4 software (Applied Biosystems). Forward and reverse primer sequences for mouse *18S* rRNA, *Cxcl1*, *Cxcl2*, *Il6*, *Il11*, *Il17a*, *Il17f*, *Socs3* and *Vegf*, and human *IL6* have been previously published (38, 39). Sequences for other mouse and human primers are presented in Supplementary Table S2.

Statistical analyses

Statistics were generated using GraphPad Prism for Windows version 5.0, and where appropriate parametric (one-way ANOVA, Student *t* test) or nonparametric (Kruskal Wallis, Mann–Whitney) tests were used. P value of <0.05 was considered statistically significant. Data are expressed as the mean ± SEM.

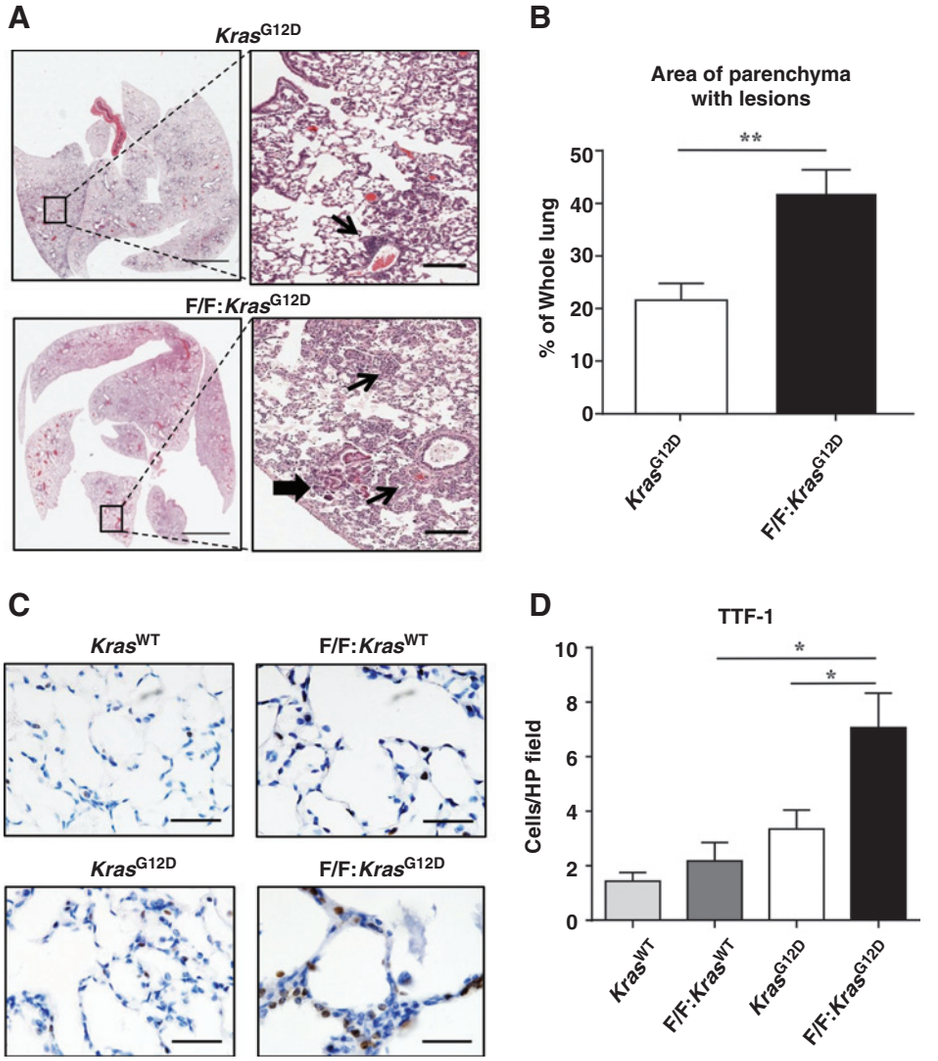

Figure 1.
Augmented Kras-induced lung adenocarcinoma in *gp130*$^{F/F}$ mice. A, representative low-power (left) and high-power (right) photomicrographs showing H&E-stained lung cross-sections from *gp130*$^{+/+}$:*Kras*$^{G12D/+}$ and *gp130*$^{F/F}$:*Kras*$^{G12D/+}$ mice administered with adenoCre virus (*Kras*^{G12D} and F/F:*Kras*^{G12D}, respectively) for 6 weeks. Small arrows, discrete AIS lesions. Large arrow, an invasive AIS lesion. Scale bars, 3 mm (left) and 300 μm (right). B, quantification of lung parenchyma area occupied by AIS lesions. Data from 6 to 9 mice per group are expressed as mean ± SEM. **, $P < 0.01$. C, representative high-power photomicrographs of TTF-1–stained lung cross-sections from *Kras*^{G12D} and F/F:*Kras*^{G12D} mice, and control *gp130*$^{+/+}$:*Kras*$^{G12D/+}$ and *gp130*$^{F/F}$:*Kras*$^{G12D/+}$ mice administered with vehicle (*Kras*^{WT} and F/F:*Kras*^{WT}, respectively) for 6 weeks. Scale bar, 50 μm. D, quantification of TTF-1–positive cells per high-power (HP) field in lungs of the indicated mice, and data are presented as the mean ± SEM from 4 to 8 mice per group. *, $P < 0.05$.

Results

Exacerbated adenocarcinoma *in situ* in the lungs of *gp130*$^{F/F}$:*Kras*^{G12D} mice

The *gp130*$^{F/F}$ mice were back-crossed onto the *Kras*$^{G12D/+}$ background, following which, activation of oncogenic *Kras*^{G12D} specifically within the lung epithelium of 6-week-old mice was initiated upon intranasal administration of adenoviral Cre recombinase. At 6 weeks after oncogenic Kras^{G12D} activation, histopathologic evaluation of H&E-stained sections of lungs of *Kras*^{G12D} mice revealed the presence of mild atypical adenomatous hyperplasia (AAH) together with small, sporadic adenocarcinoma *in situ* (AIS) lesions, consistent with previous observations (Fig. 1A; refs. 7, 40). By contrast, extensive AAH, diffuse AIS, and areas of invasive adenocarcinoma were observed throughout the lungs of *gp130*$^{F/F}$:*Kras*^{G12D} mice, and there was an overall significant 2-fold increase in the area of lung parenchyma affected by these lesions in *gp130*$^{F/F}$:*Kras*^{G12D} compared with *Kras*^{G12D} mice (Fig. 1A and B). No such lesions were observed in the lungs of control *gp130*$^{F/F}$:*Kras*$^{G12D/+}$ and *Kras*$^{G12D/+}$ mice expressing wild-type *Kras* (*Kras*^{WT}), which were subjected to intranasal inhalation with PBS vehicle (data not shown). In support of the exacerbated lung tumorigenesis in *gp130*$^{F/F}$:*Kras*^{G12D} mice, immunohistochemical evaluation with the alveolar epithelial type II cell marker TTF-1, which is used for the clinical diagnosis of lung adenocarcinoma (41), indicated a significant 2-fold increase in the number of TTF-1–positive (TTF-1^{+}) cells in *gp130*$^{F/F}$:*Kras*^{G12D} compared with *Kras*^{G12D} lungs (Fig. 1C and D). Thus, these data demonstrate that deregulated gp130-dependent signaling augments Kras^{G12D}-induced lung carcinogenesis.

Exacerbated lung carcinogenesis in *gp130*$^{F/F}$:*Kras*^{G12D} mice is associated with augmented lung cellular proliferation

The role of inflammation in Kras-induced lung carcinogenesis remains unclear, with conflicting reports regarding the extent of pulmonary inflammation elicited upon oncogenic *Kras*^{G12D} activation within the lung epithelium in mice (7, 17, 42). We observed a comparable increase in the number of CD45^{+} immune cells in the lungs of both *gp130*$^{F/F}$:*Kras*^{G12D} and *Kras*^{G12D} mice compared with control tumor-free *gp130*$^{F/F}$:*Kras*^{WT} and *Kras*^{WT} mice, respectively (Supplementary Fig. S1A and S1B). Therefore,

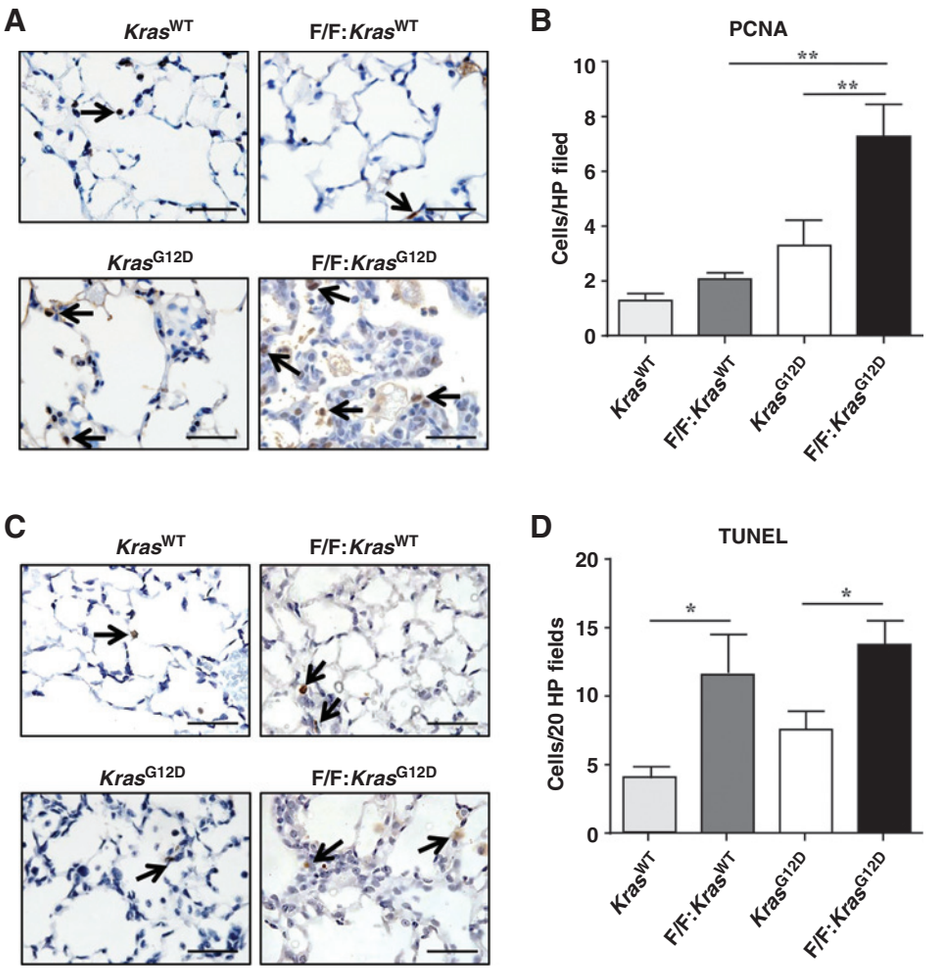

Figure 2.
Elevated cellular proliferation is associated with augmented Kras^{G12D}-induced lung adenocarcinoma in *gp130*$^{F/F}$ mice. A and C, representative photomicrographs of lung cross-sections from *Kras*^{G12D} and F/F:*Kras*^{G12D} mice, or control *Kras*^{WT} and F/F:*Kras*^{WT} mice that were subjected to PCNA staining (A) and TUNEL assay (C). Arrows, positively stained cells. Scale bars, 50 μm. B and D, quantitative enumeration of PCNA (B)- and TUNEL (D)-positive cells, respectively, per high-power (HP) field. Data are presented as the mean ± SEM from 4 to 12 mice per group. *, $P < 0.05$; **, $P < 0.01$.

although these data suggest that oncogenic Kras within the lung epithelium can elicit pulmonary inflammation, this is however not associated with the exacerbated lung tumorigenesis observed in *gp130*$^{F/F}$:*Kras*^{G12D} mice.

Because a key cellular process implicated in Kras^{G12D}-driven lung carcinogenesis is proliferation, we next examined whether the exacerbated lung tumorigenesis in *gp130*$^{F/F}$:*Kras*^{G12D} mice correlated with a higher proliferative potential in the lung. Indeed, there was a significant 3.5-fold and 2-fold increase in the number of PCNA^{+} cells throughout the lungs (i.e., both normal and tumor tissue) of *gp130*$^{F/F}$:*Kras*^{G12D} mice compared with control *gp130*$^{F/F}$:*Kras*^{WT} and *Kras*^{G12D} mice, respectively (Fig. 2A and B). By contrast, and consistent with previous observations for the *Kras*^{G12D} lung adenocarcinoma model (17, 39), the numbers of apoptotic TUNEL^{+} cells in the lungs of either *gp130*$^{F/F}$:*Kras*^{G12D} or *Kras*^{G12D} mice compared with their *Kras*^{WT} controls were unchanged (Fig. 2C and D). In this regard, although there was a significant increase in the number of apoptotic cells in the lungs of *gp130*$^{F/F}$:*Kras*^{G12D} compared with *Kras*^{G12D} mice as reported previously, this is also observed in *gp130*$^{F/F}$ compared with *gp130*$^{+/+}$ mice with wild-type *Kras* (30), and thus is independent of their *Kras* mutational status.

We next explored whether the exacerbated lung tumorigenesis in *gp130*$^{F/F}$:*Kras*^{G12D} mice was associated with upregulated expression of genes encoding key angiogenic factors VEGF, matrix metalloproteinases 2 and 9, and the glutamic acid–leucine–arginine (ELR) motif-containing chemokines CXCL-1 and CXCL-2 (43). However, the expression of these genes was comparable between *gp130*$^{F/F}$:*Kras*^{G12D} and *Kras*^{G12D} mice (Supplementary Fig. S2). These data therefore suggest that deregulated gp130 signaling coupled with oncogenic Kras within the lung epithelium selectively modulates the proliferative responsiveness of tumor cells.

Increased IL6 production and STAT3 activation are associated with exacerbated lung carcinogenesis in *gp130*$^{F/F}$:*Kras*^{G12D} mice

To examine whether the exacerbated lung adenocarcinoma phenotype of *gp130*$^{F/F}$:*Kras*^{G12D} mice was linked to deregulated expression of specific members of the IL6 cytokine family, qPCR was used to measure the mRNA levels of IL6 family cytokines during Kras^{G12D}-induced lung carcinogenesis. Among the IL6 family cytokines examined, as well as other cytokines with overlapping biologic activities such as IL17, only the expression of the *Il6* gene was significantly elevated in *gp130*$^{F/F}$:*Kras*^{G12D} mouse lungs (Fig. 3A and data not shown). Furthermore, ELISA on lung lysates revealed that IL6 protein levels were significantly elevated in *gp130*$^{F/F}$:*Kras*^{G12D} mouse lungs (Fig. 3B). Based on these findings, we next generated *gp130*$^{F/F}$:*Kras*^{G12D}:*Il6*$^{-/-}$ mice to explore

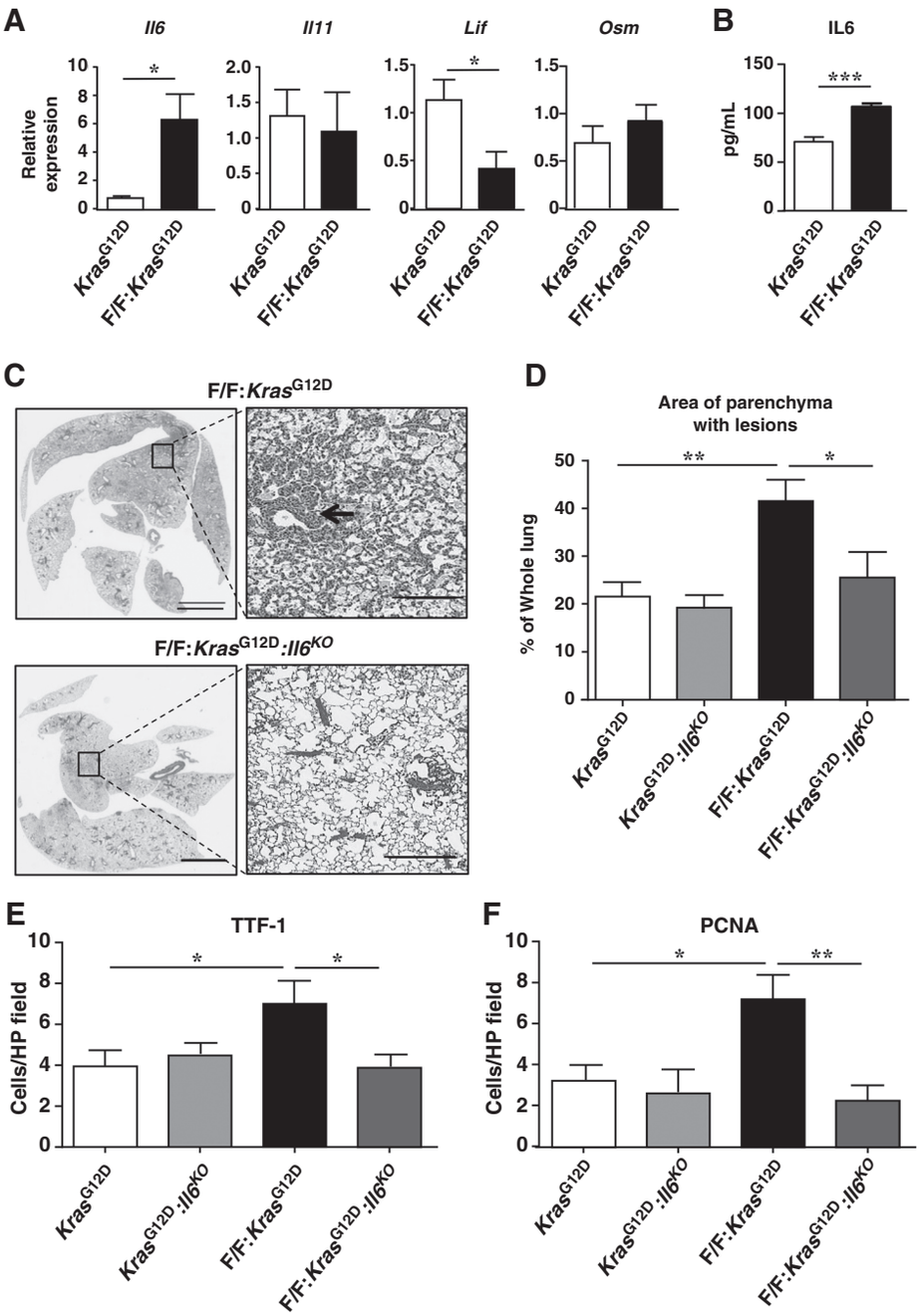

Figure 3.
IL6 deficiency in *gp130*$^{F/F}$ mice suppresses Kras^{G12D}-induced lung adenocarcinoma. A, qPCR gene expression analyses on lung cDNA from *Kras*^{G12D} and F/F:*Kras*^{G12D} mice. Expression data are normalized against *18S* and are presented from 5 to 7 mice per group as the mean ± SEM. *, $P < 0.05$. B, ELISA for IL6 on lung lysates from the indicated mice, and data are presented from 5 to 8 mice per group as the mean ± SEM. **, $P < 0.001$. C, representative low-power (left) and high-power (right) photomicrographs showing H&E-stained lung cross-sections from the indicated mice. Arrow, a discrete AIS lesion. Scale bars, 3 mm (left) and 300 μm (right). D, quantification of lung parenchyma area occupied by AIS lesions. Data from 6 to 9 mice per group are expressed as mean ± SEM. *, $P < 0.05$; **, $P < 0.01$. E and F, quantification of TTF-1 (E)– and PCNA (F)-positive cells, respectively, per high-power (HP) field in lungs of the indicated mice. Data are presented as the mean ± SEM from 6 to 9 mice per group. *, $P < 0.05$; **, $P < 0.01$.

whether IL6 deficiency would suppress the severity of the lung adenocarcinoma phenotype in *gp130*$^{F/F}$:*Kras*^{G12D} mice. Indeed, the area of lung parenchyma–containing AAH and AIS lesions in *gp130*$^{F/F}$:*Kras*^{G12D}:*Il6*$^{-/-}$ mice was significantly reduced compared with *gp130*$^{F/F}$:*Kras*^{G12D} mice (Fig. 3C and D), and was associated with significant reductions in TTF-1^{+} and PCNA^{+} cell numbers (Fig. 3E and F), as well as TUNEL^{+} and CD45^{+} cells (Supplementary Fig. S3). By contrast, IL6 deficiency in *Kras*^{G12D}:*Il6*$^{-/-}$ mice after 6 weeks of Kras oncogenic activation did not suppress lung carcinogenesis (Fig. 3D–F). These data therefore confirm that augmented IL6 expression can potentiate lung adenocarcinoma in *gp130*$^{F/F}$:*Kras*^{G12D} mice.

We have previously demonstrated that genetic ablation of IL6 in the lungs of *gp130*$^{F/F}$ mice normalizes the activation levels of STAT3 (32), whose hyper-activation is a common feature of human lung adenocarcinoma (20, 44). Consistent with this latter observation, expression of the STAT3 target gene *Socs3*, which is a *bona fide* read-out for STAT3 activity, is augmented in the lungs of *gp130*$^{F/F}$:*Kras*^{G12D} mice (Fig. 4A), and nuclear staining of pY-STAT3 is frequently observed in epithelial cells within lesions

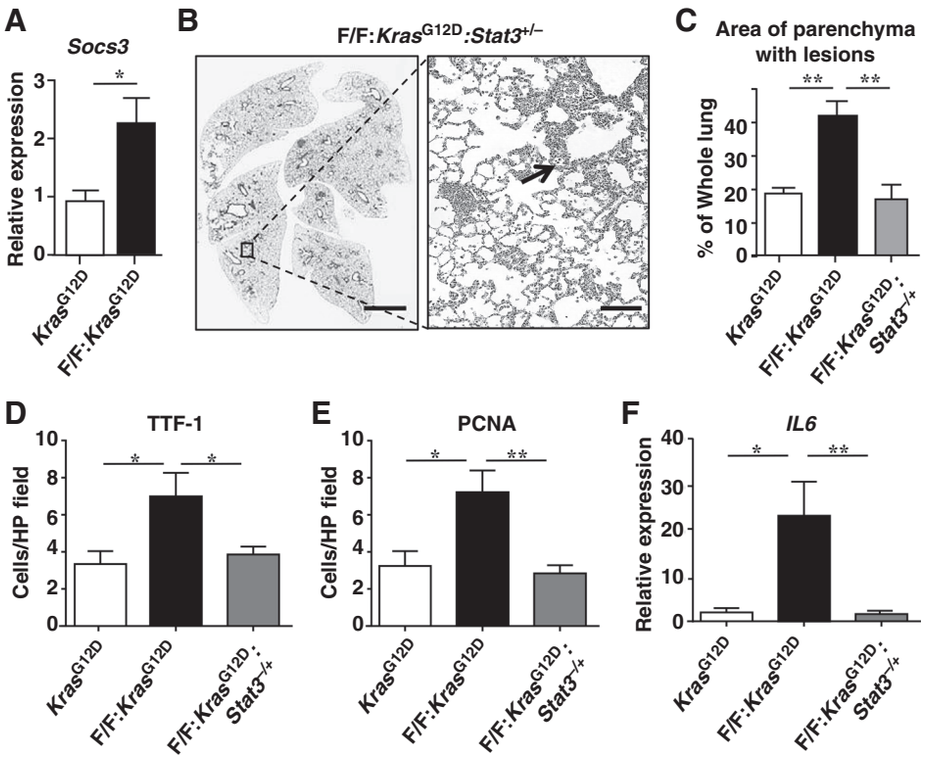

Figure 4.

Heterozygous ablation of *Stat3* in *gp130*$^{F/F}$ mice suppresses Kras^{G12D}-induced lung adenocarcinoma. A, qPCR for *Socs3* on lung cDNA from *Kras*^{G12D} and F/F:*Kras*^{G12D} mice for 6 weeks. Expression data are normalized against *18S* and are presented from 5 to 7 mice per group as the mean ± SEM. *, $P < 0.05$. B, representative low-power (left) and high-power (right) photomicrographs showing H&E-stained lung cross-sections from *gp130*$^{+/+}$:*Kras*$^{G12D/+}$:*Stat3*$^{-/+}$ mice administered with adenoCre virus (F/F:*Kras*^{G12D} *Stat3*$^{-/+}$) for 6 weeks. Arrow, a small lesion. Scale bars, 3 mm (left) and 300 μm (right). C, quantification of lung parenchyma area occupied by AIS lesions. Data from 5 to 8 mice per group are expressed as mean ± SEM. **, $P < 0.05$. D and E, quantification of TTF-1 (D)– and PCNA (E)-positive cells, respectively, per high-power (HP) field in lungs of the indicated mice. Data are presented as the mean ± SEM from 6 to 9 mice per group. *, $P < 0.05$; **, $P < 0.01$. F, qPCR for *Il6* on lung cDNA from the indicated mice. Expression data are normalized against *18S* and are presented from 5 to 7 mice per group as the mean ± SEM. *, $P < 0.05$; **, $P < 0.01$.

of *gp130*$^{F/F}$:*Kras*^{G12D} mouse lungs (Supplementary Fig. S4). To further examine whether STAT3 hyper-activation in *gp130*$^{F/F}$ mice exacerbated Kras^{G12D}-induced lung adenocarcinoma, we crossed *gp130*$^{F/F}$:*Stat3*$^{-/+}$ mice displaying normalized pulmonary STAT3 activation levels (32) with *Kras*^{G12D} mice. The development of lung adenocarcinoma in *gp130*$^{F/F}$:*Kras*^{G12D}:*Stat3*$^{-/+}$ mice was significantly reduced, similar to that observed in *Kras*^{G12D} mice, and was associated with significantly lower numbers of TTF-1^{+} and PCNA^{+} cells in the lung (Fig. 4B–E). Furthermore, the suppressed lung adenocarcinoma in *gp130*$^{F/F}$:*Kras*^{G12D}:*Stat3*$^{-/+}$ mice was marked by a significant reduction in *Il6* mRNA levels (Fig. 4F). Thus, these data support the notion that IL6/gp130/STAT3 hyper-activation can potentiate Kras^{G12D}-induced lung adenocarcinoma, and also invoke the existence of a possible feed-forward loop whereby gp130/STAT3 hyper-activation augments the transcriptional induction of IL6.

IL6 trans-signaling exacerbates lung carcinogenesis in *gp130*$^{F/F}$:*Kras*^{G12D} mice

At 6 weeks after activation of oncogenic *Kras* in the lung epithelium, both ELISA and immunoblotting demonstrated augmented protein levels of sIL6R, the key driver of IL6 trans-signaling, in lung lysates from *gp130*$^{F/F}$:*Kras*^{G12D} compared with *Kras*^{G12D} mice (Fig. 5A and B). By contrast, protein levels of sgp130, the naturally occurring antagonist of IL6 trans-signaling, were unchanged. To examine whether IL6 trans-signaling promoted the exacerbated lung adenocarcinoma phenotype in *gp130*$^{F/F}$:*Kras*^{G12D} mice, we crossed *gp130*$^{F/F}$:*Kras*^{G12D} mice with transgenic *sgp130Fc*^{Tg} mice that systemically express sgp130Fc, a fusion protein of sgp130 and the Fc portion of human IgG1, which serves as a specific and potent IL6 trans-signaling inhibitor (33). The sgp130Fc-mediated blockade of IL6 trans-signaling in lungs of *gp130*$^{F/F}$:*Kras*^{G12D}:*sgp130Fc*^{Tg} mice reduced STAT3 activity by approximately 30% (Supplementary Fig. S5) and, importantly, suppressed the extent of AAH and AIS lesion development compared with *gp130*$^{F/F}$:*Kras*^{G12D} mice, which was associated with reduced numbers of TTF-1^{+} and PCNA^{+} cells (Fig. 5C–F). Although the mild lung adenocarcinoma phenotype of *Kras*^{G12D} mice was alleviated in *Kras*^{G12D}:*sgp130Fc*^{Tg} mice, this was not significant (Fig. 5C–F).

To further determine whether IL6 trans-signaling can serve as a *bona fide* therapeutic target for Kras^{G12D}-driven lung adenocarcinoma, we next treated *gp130*$^{F/F}$:*Kras*^{G12D} mice over the course of 6 weeks with 2 anti-IL6R mAbs, 25F10 and 1F7

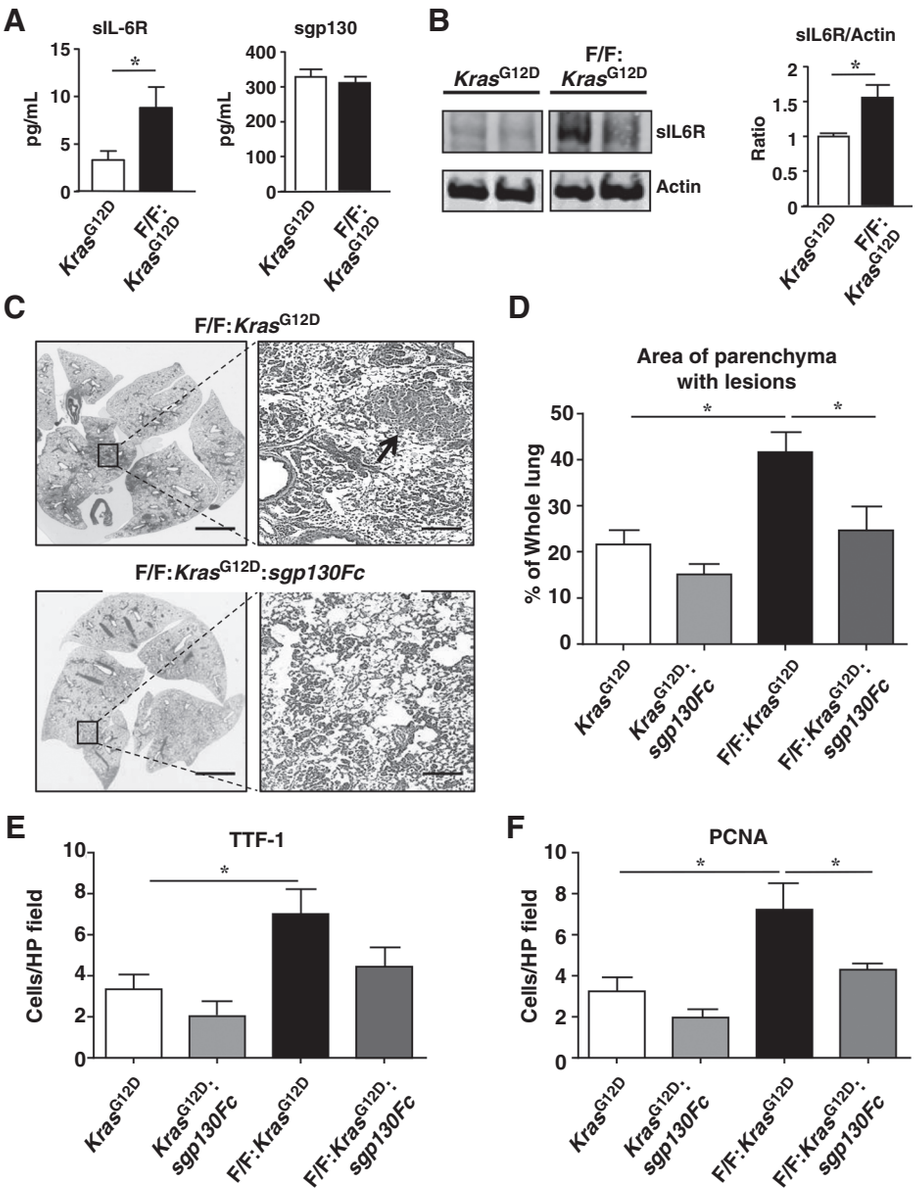

Figure 5.
Genetic ablation of IL6 trans-signaling with sgp130Fc in *gp130*$^{F/F}$ mice suppresses Kras^{G12D}-induced lung adenocarcinoma. A, ELISA for sIL6R and sgp130 on lung lysates from *Kras*^{G12D} and F/F:*Kras*^{G12D} mice. Data are presented from 5 mice per group as the mean ± SEM. *, $P < 0.05$. B, immunoblots of representative *Kras*^{G12D} and F/F:*Kras*^{G12D} lung lysates with antibodies against sIL6R (50 kDa) and actin. Graph depicts densitometric semiquantitative analysis of sIL6R protein levels in three lung lysates per genotype, and relative expression was determined against actin. *, $P < 0.05$. C, representative low-power (left) and high-power (right) photomicrographs showing H&E-stained lung cross-sections from the indicated mice. Arrow, a discrete AIS lesion. Scale bars, 3 mm (left) and 300 μm (right). D, quantification of lung parenchyma area occupied by AIS lesions. Data from 6 to 9 mice per group are expressed as mean ± SEM. *, $P < 0.05$. E and F, quantification of TTF-1 (E)– and PCNA (F)-positive cells, respectively, per high-power (HP) field in the lungs of the indicated mice. Data are presented as the mean ± SEM from 5 to 9 mice per group. *, $P < 0.05$.

(which efficiently block IL6 trans-signaling in the mouse; refs. 35, 36). The treatment of *gp130*$^{F/F}$:*Kras*^{G12D} mice with either 25F10 or 1F7 significantly suppressed the identical exacerbated lung adenocarcinoma phenotype observed in both isotype control antibody-treated and untreated *gp130*$^{F/F}$:*Kras*^{G12D} mice (Fig. 6A and B). Consistent with these observations, TTF-1^{+} and PCNA^{+} cell numbers were also reduced in the lungs of *gp130*$^{F/F}$:*Kras*^{G12D} mice treated with either 25F10 or 1F7 (Fig. 6C and D). Interestingly, significantly lower numbers of TTF-1^{+} and PCNA^{+} cells were also present in the lungs of *Kras*^{G12D} mice treated with 1F7 compared with isotype control, and this was associated with a reduction in the area of lung parenchyma–containing lesions, albeit not significant (Supplementary Fig. S6). Collectively, these data reveal that blockade of IL6 trans-signaling suppresses *Kras*^{G12D}-driven lung carcinogenesis.

Upregulation of IL6 trans-signaling components in human lung adenocarcinoma

In lung tissues of lung adenocarcinoma patients (Supplementary Table S1), mRNA levels for *SOCS3*, whose expression is indicative of STAT3 activity, were increased 4-fold compared with control individuals (Fig. 7A). Among IL6 family cytokines, only mRNA levels for *IL6* were significantly increased (13-fold) in lung adenocarcinoma patients (Fig. 7A). Furthermore, IL6 and sIL6R protein levels were significantly elevated in lung lysates (Fig. 7B) and serum (Fig. 7C) from lung adenocarcinoma patients, and displayed a positive correlation with each other (Fig. 7D).

To further investigate the involvement of IL6 trans-signaling in human lung adenocarcinoma, we first confirmed that IL6 and sIL6R protein levels were readily detectable in culture supernatants of 2 independent human *KRAS* mutant cell lines, A549 and H23 (Supplementary Fig. S7A). Next, we assessed whether specific

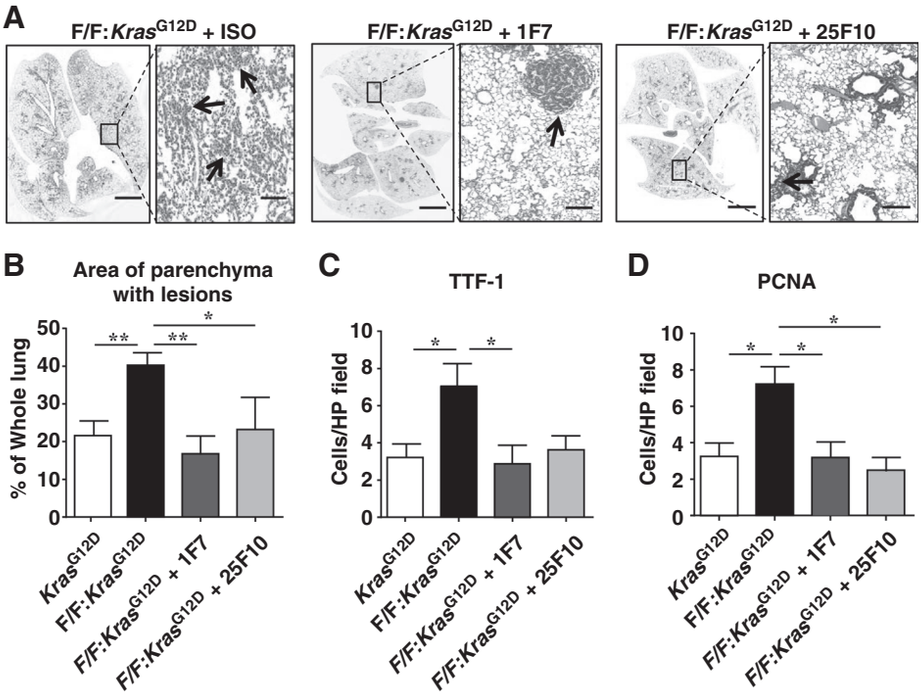

Figure 6.
Antibody-mediated blockade of IL6 trans-signaling in *gp130*$^{F/F}$ mice suppresses Kras^{G12D}-induced lung adenocarcinoma. A, representative low-power (left) and high-power (right) photomicrographs showing H&E-stained lung cross-sections from F/F:*Kras*^{G12D} mice treated with either 1F7, 25F10, or isotype control (ISO) mAbs for 6 weeks. Arrows, AIS lesions. Scale bars, 3 mm (left) and 300 μm (right). B, quantification of the area of lung parenchyma occupied by AIS lesions. Note that the "F/F:*Kras*^{G12D}" mouse group comprises untreated and ISO-treated mice since the exacerbated lung adenocarcinoma phenotype was histologically identical among these two groups. Data from 4 to 8 mice per group are expressed as mean ± SEM. *, $P < 0.05$; **, $P < 0.01$. C and D, quantification of TTF-1 (C)– and PCNA (D)-positive cells, respectively, per high-power (HP) field in lungs of the indicated mice. Data are presented as the mean ± SEM from 3 to 5 mice per group. *, $P < 0.05$.

blockade of IL6 trans-signaling upon treatment of these cell lines with sgp130Fc (which also acts on human cells) would negate their growth in cell culture. Indeed, MTT assays revealed that sgp130Fc significantly suppressed the growth of both A549 and H23 cell lines compared with control vehicle–treated cells (Supplementary Fig. S7B). Taken together, these data support a role for IL6 trans-signaling in the pathogenesis of human lung adenocarcinoma.

Discussion

A role for IL6 family cytokines in the pathogenesis of lung adenocarcinoma has been suggested by both clinical data demonstrating that IL6 levels are augmented in human lung adenocarcinoma patients (19–21), as well as an oncogenic *Kras*^{G12D}-driven mouse lung adenocarcinoma model whereby genetic ablation of IL6 alleviates lung tumorigenesis (18). Despite these observations, the involvement of other members of the IL6 cytokine family in Kras-driven lung carcinogenesis, as well as the mode of signaling by which IL6 promotes lung adenocarcinoma, remains unknown. Here, we reveal for the first time that among IL6 family cytokines, augmented levels of only IL6 and its essential trans-signaling receptor subunit, sIL6R, are observed in lung adenocarcinoma patients, and also are associated with exacerbated Kras^{G12D}-driven lung carcinogenesis in mice.

Despite the comparable high levels of naturally occurring sgp130 in the lungs of both *Kras*^{G12D} and *gp130*$^{F/F}$:*Kras*^{G12D} mice, the 2-fold increase in sIL6R levels in *gp130*$^{F/F}$:*Kras*^{G12D} mouse lungs, without any increase in sgp130 levels, means that (on a molar basis) endogenous sgp130 levels are insufficient to block pathologic trans-signaling (10). This is in contrast with the administration of sgp130Fc, which is approximately 10 to 100 times more effective than sgp130 alone at blocking IL6 trans-signaling (45). Indeed, the amelioration of the exacerbated lung adenocarcinoma phenotype in *gp130*$^{F/F}$:*Kras*^{G12D} mice upon transgenic overexpression of sgp130Fc is of potential clinical significance since sgp130Fc has already successfully completed phase I clinical trials, and will undergo future phase II clinical trials in Europe in patients with inflammatory bowel disease (46). We also demonstrate here that the sgp130Fc-mediated blockade of IL6 trans-signaling suppressed the growth of human lung adenocarcinoma cell lines. Recently, siltuximab, a chimeric mouse/human mAb that binds to and neutralizes human IL6 (i.e., blocks classical and trans-signaling), has shown promise in inhibiting the growth of tumors in preclinical lung adenocarcinoma cell line xenograft models (47). In addition, preliminary trials using a humanized neutralizing mAb against IL6, ALD-518, which like siltuximab targets "global" IL6 signaling, has shown promise in ameliorating fatigue and cachexia associated with advanced metastatic non–small cell lung cancer, although the antitumor effects of such therapy were not reported (48). Although the efficacy of using such global anti-IL6 signaling mAbs to suppress tumor growth in lung adenocarcinoma patients remains unknown, an inherent issue that may arise involves targeting "immune-protective" IL6 classical signaling. Indeed, a common drawback associated with global anti-IL6 therapeutics is the numerous adverse events, especially infections, which are most likely a consequence of suppressing the ability of classical IL6 signaling to protect the host against bacterial infections due to an impaired hepatic acute phase response. Our data presented here showing that two anti-IL6R mAbs, which act in the mouse to target trans-signaling, can reduce the severity of Kras^{G12D}-induced lung adenocarcinoma, indicating that humanized variants of such mAbs could provide a rational therapeutic approach for human lung adenocarcinoma patients displaying augmented IL6 (and sIL6R) levels.

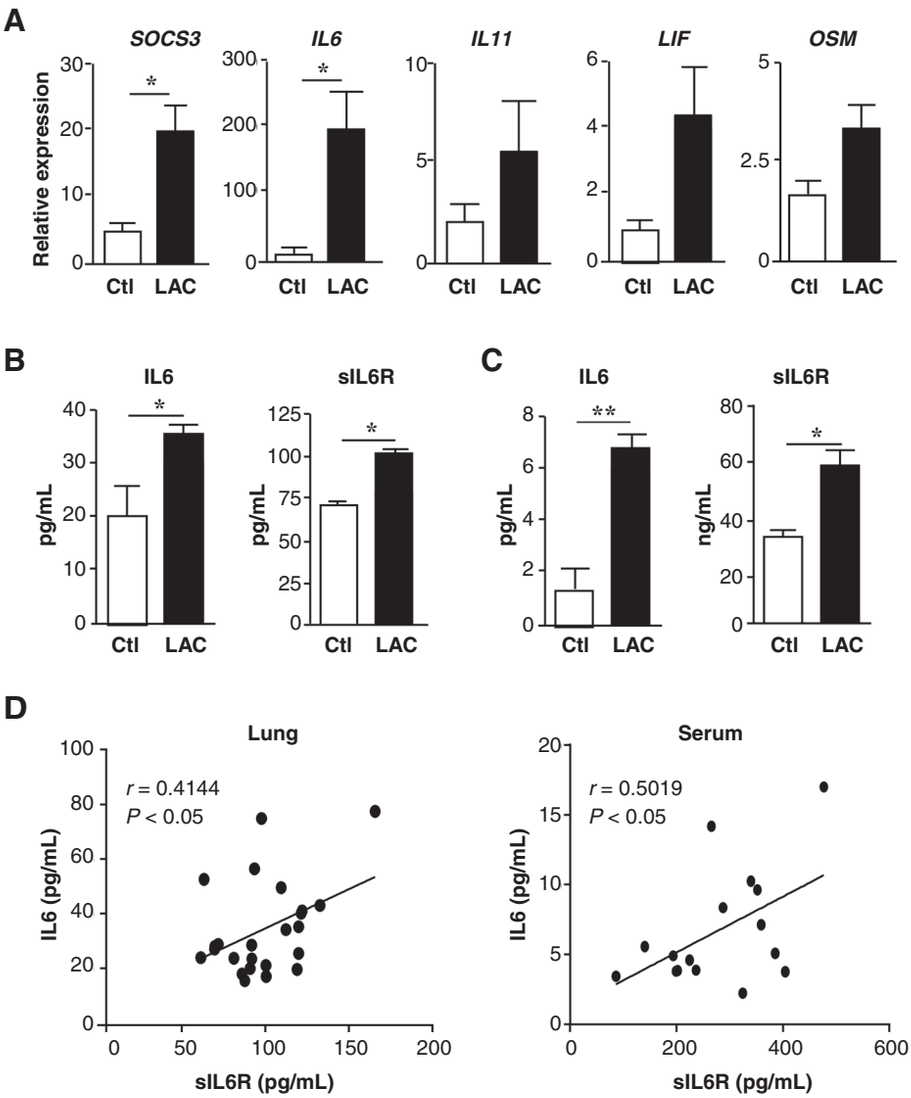

Figure 7.
Augmented levels of IL6 trans-signaling components in human lung adenocarcinoma (LAC) tissue and serum. A, qPCR gene expression analyses in human lung cDNA from lung adenocarcinoma patients ($n = 24$) or control (Ctl) lung adenocarcinoma–free individuals ($n = 5$). Expression data are normalized for *18S* expression and are presented from triplicate analysis as the mean ± SEM. *, $P < 0.05$. B and C, IL6 and sIL6R protein concentrations in lung lysates (B) and serum (C) from control and lung adenocarcinoma groups were determined by ELISA. Data are expressed as the mean ± SEM. *, $P < 0.05$; **, $P < 0.01$. D, linear regression analyses of IL6 and sIL6R protein expression in lung lysates and serum from lung adenocarcinoma patients. *r*, Pearson correlation coefficient.

Although the downstream mediators of Kras-induced lung adenocarcinoma remain ill-defined, our data here suggest that enhanced activation of STAT3 (via IL6 trans-signaling, and as occurs in $gp130^{F/F}$ mice) can augment the oncogenic potency of the activating $Kras^{G12D}$ mutant. The combined observations that tyrosine-phosphorylated (i.e., activated) STAT3 resides primarily in the respiratory epithelium (where the oncogenic $Kras^{G12D}$ mutant is expressed from its endogenous promoter) of $gp130^{F/F}$:$Kras^{G12D}$ mouse lungs, and the exacerbated lung adenocarcinoma phenotype in $gp130^{F/F}$:$Kras^{G12D}$ mice is not associated with any further increase in leukocyte infiltrates, support the notion that gp130(Y757F)-dependent oncogenic cellular responses in the lung are driven by the epithelium, as we have reported previously for the epithelium of other tissues from $gp130^{F/F}$ mice, such as the stomach (39). We also note that our current findings are consistent with the previous report that IL6 trans-signaling and STAT3 are required for tumorigenesis in a $Kras^{G12D}$-induced pancreatic adenocarcinoma mouse model (16). Furthermore, autocrine IL6/STAT3 signaling can promote the *KRAS*-dependent cell survival and proliferation *in vitro* of human lung adenocarcinoma cell lines, although the specific role of IL6 trans-signaling was not addressed (9). In addition, IL6 has been shown to be required for Ras-driven tumorigenesis in multiple cell types; however, its role in lung adenocarcinoma was not investigated (49).

Although collectively these observations imply that STAT3 via IL6 trans-signaling can augment the oncogenic potential of mutant Kras in lung adenocarcinoma, recently it was reported that the lung epithelial-specific inactivation of *Stat3* exacerbates $Kras^{G12D}$-driven lung adenocarcinoma (40). The tumor-suppressive activity of STAT3 was assigned to its ability to sequester cytoplasmic NF-κB and inhibit NF-κB–induced transcription of the proangiogenic chemokine *Cxcl1*, thus suppressing tumor vascularization and growth. Although the upstream STAT3-activating cytokines responsible for the tumor-suppressive activity of STAT3 were not identified, these findings are reminiscent of previous studies using *Stat3* conditional ablation in mice, which invariably block the anti-inflammatory and

tumor-suppressive action of IL10, which activates STAT3 homodimers (50). In this respect, it is therefore not surprising that *Cxcl1* gene expression was unchanged in the lungs of $gp130^{F/F}$:$Kras^{G12D}$ mice displaying exacerbated lung adenocarcinoma compared with $Kras^{G12D}$ mice, because IL6 trans-signaling also activates STAT3 heterodimers with STAT1 (13, 25), thus modulating a different network of gene targets compared with that modulated by other cytokines, such as IL-10, which activates STAT3 homodimers.

In conclusion, our mouse model data revealing that specific targeting of IL6 trans-signaling (when IL6 is overexpressed) suppresses lung adenocarcinoma pathogenesis, together with clinical data showing positive correlations between elevated sIL6R and IL6 levels in tumors and sera of lung adenocarcinoma patients, have translational potential for biomarker discovery and early disease detection, as well as patient stratification for potential responders that may benefit from selective anti-IL6 trans-signaling therapies. Based on our findings, it will now be of interest to examine whether IL6 trans-signaling contributes to the pathogenesis of KRAS-independent lung cancer subtypes (e.g., small cell lung cancer) in which IL6 has been implicated.

Disclosure of Potential Conflicts of Interest

S. Rose-John has ownership interest (including patents) in stocks and patents; and is a consultant/advisory board member for AbbVie, Chugai, Janssen, and Roche. No potential conflicts of interest were disclosed by the other authors.

Authors' Contributions

Conception and design: S. Rose-John, S. Ruwanpura, B.J. Jenkins
Development of methodology: G.D. Brooks, A. Miller, P.A. Russell, S. Rose-John, S. Ruwanpura, B.J. Jenkins
Acquisition of data (provided animals, acquired and managed patients, provided facilities, etc.): G.D. Brooks, L. McLeod, A. Miller, P.A. Russell, S. Rose-John, B.J. Jenkins
Analysis and interpretation of data (e.g., statistical analysis, biostatistics, computational analysis): G.D. Brooks, L. McLeod, P.A. Russell, S. Rose-John, S. Ruwanpura, B.J. Jenkins
Writing, review, and/or revision of the manuscript: G.D. Brooks, P.A. Russell, W. Ferlin, S. Rose-John, B.J. Jenkins
Administrative, technical, or material support (i.e., reporting or organizing data, constructing databases): G.D. Brooks, L. McLeod, S. Alhayyani, S. Ruwanpura
Study supervision: S. Ruwanpura, B.J. Jenkins

Grant Support

This work was supported by the National Health and Medical Research Council (NHMRC) of Australia, as well as the Operational Infrastructure Support Program by the Victorian Government of Australia. S.Ruwanpura is supported by an NHMRC Post-doctoral Training Fellowship. S. Rose-John is supported by grants from the Deutsche Forschungsgemeinschaft, Bonn, Germany (SFB841, project C1; SFB877 project A1) and by the Cluster of Excellence "Inflammation at Interfaces." B.J. Jenkins is supported by an NHMRC Senior Medical Research Fellowship.

The costs of publication of this article were defrayed in part by the payment of page charges. This article must therefore be hereby marked *advertisement* in accordance with 18 U.S.C. Section 1734 solely to indicate this fact.

Received August 26, 2015; revised November 17, 2015; accepted December 6, 2015; published OnlineFirst January 7, 2016.

References

1. Jemal A, Bray F, Center MM, Ferlay J, Ward E, Forman D. Global cancer statistics. CA Cancer J Clin 2011;61:69–90.
2. Walser T, Cui X, Yanagawa J, Lee JM, Heinrich E, Lee G, et al. Smoking and lung cancer: the role of inflammation. Proc Am Thorac Soc 2008;5:811–5.
3. Gerber DE. EGFR inhibition in the treatment of non-small cell lung cancer. Drug Dev Res 2008;69:359–72.
4. Ahrendt S, Decker PA, Alawi EA, Zhu YR, Sanchez-Cespedes M, Yang SC, et al. Cigarette smoking is strongly associated with mutation of the K-ras gene in patients with primary adenocarcinoma of the lung. Cancer 2001 92:1525–30.
5. Brose MS, Volpe P, Feldman M, Kumar M, Rishi I, Gerrero R, et al. BRAF and RAS mutations in human lung cancer and melanoma. Cancer Res 2002; 62:6997–7000.
6. Riely GJ, Kris MG, Rosenbaum D, Marks J, Li A, Chitale DA, et al. Frequency and distinctive spectrum of KRAS mutations in never smokers with lung adenocarcinoma. Clin Cancer Res 2008;14:5731–4.
7. Jackson E, Willis N, Mercer K, Bronson RT, Crowley D, Montoya R, et al. Analysis of lung tumor initiation and progression using conditional expression of oncogenic K-ras. Genes Dev 2001;15:3243–8.
8. DuPage M, Dooley AL, Jacks T. Conditional mouse lung cancer models using adenoviral or lentiviral delivery of Cre recombinase. Nat Protoc 2009;4:1064–72.
9. Zhu Z, Aref AR, Cohoon TJ, Barbie TU, Imamura Y, Yang S, et al. Inhibition of KRAS-driven tumorigenicity by interruption of an autocrine cytokine circuit. Cancer Discov 2014;4:452–65.
10. Garbers C, Hermanns H, Schaper F, Müller-Newen G, Grötzinger J, Rose-John S, et al. Plasticity and cross-talk of interleukin 6-type cytokines. Cytokine Growth Factor Rev 2012;23:85–97.
11. Lapeire L, Hendrix A, Lambein K, Van Bockstal M, Braems G, Van Den Broecke R, et al. Cancer-associated adipose tissue promotes breast cancer progression by paracrine oncostatin M and Jak/STAT3 signaling. Cancer Res 2014;74:6806–19.
12. Sommer J, Effenberger T, Volpi E, Waetzig GH, Bernhardt M, Suthaus J, et al. Constitutively active mutant gp130 receptor protein from inflammatory hepatocellular adenoma is inhibited by an anti-gp130 antibody that specifically neutralizes interleukin 11 signaling. J Biol Chem 2012;287: 13743–51.
13. Ernst M, Najdovska M, Grail D, Lundgren-May T, Buchert M, Tye H, et al. STAT3 and STAT1 mediate IL-11-dependent and inflammation-associated gastric tumorigenesis in gp130 receptor mutant mice. J Clin Invest 2008; 118:1727–38.
14. Yu H, Yue X, Zhao Y, Li X, Wu L, Zhang C, et al. LIF negatively regulates tumor-suppressor p53 through Stat3/ID1/MDM2 in colorectal cancers. Nat Commun 2014;5:5218.
15. Grivennikov S, Karin E, Terzic J, Mucida D, Yu GY, Vallabhapurapu S, et al. IL-6 and Stat3 are required for survival of intestinal epithelial cells and development of colitis-associated cancer. Cancer Cell 2009;15:103–13.
16. Lesina M, Kurkowski MU, Ludes K, Rose-John S, Treiber M, Klöppel G, et al. Stat3/Socs3 activation by IL-6 transsignaling promotes progression of pancreatic intraepithelial neoplasia and development of pancreatic cancer. Cancer Cell 2011;19:456–69.
17. Tan X, Carretero J, Chen Z, Zhang J, Wang Y, Chen J, et al. Loss of p53 attenuates the contribution of IL-6 deletion on suppressed tumor progression and extended survival in Kras-driven murine lung cancer. PLoS One 2013;8:e80885.
18. Ochoa CE, Mirabolfathinejad S, Venado AR, Evans SE, Gagea M, Evans CM, et al. Interleukin 6, but not T helper 2 cytokines, promotes lung carcinogenesis. Cancer Prev Res 2010;4:51–64.
19. Yanagawa H, Sone S, Takahashi Y, Haku T, Yano S, Shinohara T, et al. Serum levels of interleukin 6 in patients with lung cancer. Br J Cancer 1995 71:1095–8.
20. Yeh H, Lai WW, Chen HH, Liu HS, Su WC. Autocrine IL-6-induced Stat3 activation contributes to the pathogenesis of lung adenocarcinoma and malignant pleural effusion. Oncogene 2006 25:4300–9.
21. Gao S, Mark KG, Leslie K, Pao W, Motoi N, Gerald WL, et al. Mutations in the EGFR kinase domain mediate STAT3 activation via IL-6 production in human lung adenocarcinomas. J Clin Invest 2007;117:3846–56.
22. Haura EB, Livingston S, Coppola D. Autocrine interleukin-6/interleukin-6 receptor stimulation in non-small-cell lung cancer. Clin Lung Cancer 2006;7:273–5.

23. Gomes M, Coelho A, Araújo A, Azevedo A, Teixeira AL, Catarino R, et al. IL-6 polymorphism in non-small cell lung cancer: a prognostic value? Tumor Biol 2015;36:3679–84.
24. Rose-John S, Scheller J, Elson G, Jones SA. Interleukin-6 biology is coordinated by membrane-bound and soluble receptors: role in inflammation and cancer. J Leukoc Biol 2006;80:227–36.
25. Heinrich P, Behrmann I, Haan S, Hermanns HM, Muller-Newen G, Schaper F. Principles of interleukin (IL)-6-type cytokine signaling and its regulation. Biochem J 2003;374:1–20.
26. Nowell M, Williams AS, Carty SA, Scheller J, Hayes AJ, Jones GW, et al. Therapeutic targeting of IL-6 trans signaling counteracts STAT3 control of experimental inflammatory arthritis. J Immunol 2009;182:613–22.
27. Greenhill CJ, Rose-John S, Lissilaa R, Ferlin W, Ernst M, Hertzog PJ, et al. IL-6 trans-signaling modulates TLR4-dependent inflammatory responses via STAT3. J Immunol 2011;186:1199–208.
28. Atreya R, Mudter J, Finotto S, Mullberg J, Jostock T, Wirtz S, et al. Blockade of interleukin 6 trans signaling suppresses T-cell resistance against apoptosis in chronic intestinal inflammation: evidence in crohn disease and experimental colitis in vivo. Nat Med 2000;6:583–8.
29. Becker C, Fantini MC, Schramm C, Lehr HA, Wirtz S, Nikolaev A, et al. TGF-beta suppresses tumor progression in colon cancer by inhibition of IL-6 trans-signaling. Immunity 2004;21:491–501.
30. Ruwanpura SM, McLeod L, Miller A, Jones J, Bozinovski S, Vlahos R, et al. Interleukin-6 promotes pulmonary emphysema associated with apoptosis in mice. Am J Respir Cell Mol Biol 2011;45:720–30.
31. Jenkins BJ, Grail D, Nheu T, Najdovska M, Wang B, Waring P, et al. Hyperactivation of Stat3 in gp130 mutant mice promotes gastric hyperproliferation and desensitizes TGF-beta signaling. Nat Med 2005; 11:845–52.
32. Ruwanpura SM, McLeod L, Miller A, Jones J, Vlahos R, Ramm G, et al. Deregulated Stat3 signaling dissociates pulmonary inflammation from emphysema in gp130 mutant mice. Am J Physiol Lung Cell Mol Physiol 2012;302:L627–39.
33. Rabe B, Chalaris A, May U, Waetzig GH, Seegert D, Williams AS, et al. Transgenic blockade of interleukin 6 transsignaling abrogates inflammation. Blood 2008;111:1021–8.
34. Kopf M, Baumann H, Freer G, Freudenberg M, Lamers M, Kishimoto T, et al. Impaired immune and acute-phase responses in interleukin-6-deficient mice. Nature 1994;368:339–42.
35. Lissilaa R, Buatois V, Magistrelli G, Williams AS, Jones GW, Herren S, et al. Although IL-6 trans-signaling is sufficient to drive local immune responses, classical IL-6 signaling is obligate for the induction of T cell-mediated autoimmunity. J Immunol 2010;185:5512–21.
36. Lacroix M, Rousseau F, Guilhot F, Malinge P, Magistrelli G, Herren S, et al. Novel insights into IL-6 cis- and trans-signaling pathways by differentially manipulating the assembly of the IL-6 signaling complex. J Biol Chem 2015 Sep 11. [Epub ahead of print].
37. Miller A, McLeod L, Brooks G, Ruwanpura S, Jenkins BJ. Differential involvement of gp130 signaling pathways in modulating tobacco carcinogen-induced lung tumorigenesis. Oncogene 2015;34:1510–9.
38. Kennedy CL, Najdovska M, Tye H, McLeod L, Yu L, Jarnicki A, et al. Differential role of MyD88 and Mal/TIRAP in TLR2-mediated gastric tumorigenesis. Oncogene 2014;33:2540–6.
39. Tye H, Kennedy C, Najdovska M, McLeod L, McCormack W, Hughes N, et al. STAT3-Driven Upregulation of TLR2 Promotes Gastric Tumorigenesis Independent of Tumor Inflammation. Cancer Cell 2012;22: 466–78.
40. Grabner B, Schramek D, Mueller KM, Moll HP, Svinka J, Hoffmann T, et al. Disruption of STAT3 signaling promotes KRAS-induced lung tumorigenesis. Nat Commun 2015;6:6285–98.
41. Jerome-Marson V, Mazieres J, Groussard O, Garcia O, Berjaud J, Dahan M, et al. Expression of TTF-1 and cytokeratins in primary and secondary epithelial lung tumors: correlation with histological type and grade. Histopathology 2004;45:125–34.
42. Ji H, Houghton AM, Mariani TJ, Perera S, Kim CB, Padera R, et al. K-ras activation generates an inflammatory response in lung tumors. Oncogene 2006;25:2105–12.
43. McClelland MR, Carskadon S, Zhao L, White ES, Beer DG, Orringer MB, et al. Diversity of the angiogenic phenotype in non–small cell lung cancer. Am J Respir Cell Mol Biol 2007;36:343–50.
44. Yang Q, Shen SS, Zhou S, Ni J, Chen D, Wang G, et al. STAT3 activation and aberrant ligand-dependent sonic hedgehog signaling in human pulmonary adenocarcinoma. Exp Mol Pathol 2012;93:227–36.
45. Jostock T, Müllberg J, Ozbek S, Atreya R, Blinn G, Voltz N, et al. Soluble gp130 is the natural inhibitor of soluble interleukin-6 receptor transsignaling responses. Eur J Biochem 2001;268:160–7.
46. Calabrese LH, Rose-John S. IL-6 biology: implications for clinical targeting in rheumatic disease. Nat Rev Rheumatol 2014;10:720–7.
47. Song L, Rawal B, Nemeth JA, Haura EB. JAK1 activates STAT3 activity in non-small-cell lung cancer cells and IL-6 neutralizing antibodies can suppress JAK1-STAT3 signaling. Mol Cancer Ther 2011;10:481–94.
48. Bayliss TJ, Smith JT, Schuster M, Dragnev KH, Rigas JR. A humanized anti-IL-6 antibody (ALD518) in non-small cell lung cancer. Expert Opin Biol Ther 2011;11:1663–8.
49. Ancrile B, Lim K, Counter CM. Oncogenic Ras-induced secretion of IL6 is required for tumorigenesis. Genes Dev 2007;21:1714–9.
50. Takeda K, Clausen BE, Kaisho T, Tsujimura T, Terada N, Forster I, et al. Enhanced Th1 activity and development of chronic enterocolitis in mice devoid of Stat3 in macrophages and neutrophils. Immunity 1999; 10:39–49.